applied optics

Application of point diffraction interferometry for measuring angular displacement to a sensitivity of 0.01 arcsec

D. A. Gavrilin,[1] S. V. Kuzin,[2] N. N. Salashchenko,[1] M. V. Svechnikov,[1,*] M. N. Toropov,[1] N. I. Chkhalo,[1] and A. A. Soloviev[3]

[1]Institute for Physics of Microstructures of RAS, 603950 Nizhny Novgorod, Russia
[2]Lebedev Physical Institute, 119991 Moscow, Russia
[3]Institute of Applied Physics of RAS, 603950 Nizhny Novgorod, Russia
*Corresponding author: svechnikovmv@gmail.com

Received 23 September 2015; revised 24 September 2015; accepted 29 September 2015; posted 6 October 2015 (Doc. ID 241746); published 29 October 2015

The use of point diffraction interferometry is reported for measuring minutes, on the order of 0.01 arcsec angular movements. The algorithm for determining the angular displacement by the dynamics of the interference pattern is described. We also demonstrate results for applying this method to the study of the linearity and hysteresis of the angular shift of the platform, controlled by piezo actuators, which are designed for angular adjustment of the mirror of a solar extreme-ultraviolet telescope.

OCIS codes: (120.2650) Fringe analysis; (120.3180) Interferometry; (120.4880) Optomechanics; (120.3930) Metrological instrumentation; (120.6085) Space instrumentation.

http://dx.doi.org/10.1364/AO.54.009315

1. INTRODUCTION

Currently, the Lebedev Physical Institute of the Russian Academy of Sciences is developing a telescope to study the Sun in the extreme ultraviolet (EUV) with an angular resolution of 0.1 arcsec (0.1″). The optical layout of the telescope is adapted from Ritchey–Chrétien [1]. One of the main problems during the operation of this tool is retaining the direction of the optical axis of the telescope in the selected area of the Sun with an accuracy of a few arcseconds in the area of 30 arcmin (30′) and holding it in this position during the exposure time (∼10 s) with an accuracy of about one order of magnitude greater than angular resolution, i.e., 0.01″.

In the optical layout of Ritchey–Chrétien, the implementation of this requirement is made optimal by tilting the secondary mirror. The current position of the optical axis of the telescope is controlled by high-precision optical sensors, whose signal is processed in the onboard computer of the telescope and output as control signals to the piezo actuators.

To study the basic mechanical characteristics of the tilting platform, such as the dependence of the inclination angle on the voltage of the piezo actuator, the hysteresis, and the influence of the operating and storing conditions on them, one needs a measuring instrument that provides, ideally, a measurement accuracy of an order of magnitude greater than the desired angular resolution.

In some cases, such as the development of high-precision telescopes that will work in space, the executive units, which are already integrated into the device, need to be checked in working conditions: vacuum and low temperatures. Thus, the creation of the measuring device, which enables easy integration into existing devices and working with both a large pressure and a temperature drop, is extremely important.

There are many proposed methods for measuring small angle displacement. Commercially available autocollimators can provide root-mean measurement accuracies of 0.1″ with a range of measured angles of ±12′ [2], the same level of precision achievable in other collimator schemes [3]. Autocollimation is also used in [4–6], in which the authors reported an accuracy of 0.2″ in a range of 7′, 0.05″ in ±250″, and 0.4″ in the range of ±0.2°, respectively.

Interferometric methods can significantly extend the measurement range, while maintaining accuracy, so the accuracy is 0.01″ in the range of ±0.6° in Refs. [7,8]. The effect of total external reflection is used in Refs. [9,10]; the accuracy of the method is estimated to be 0.3″ in a range of about 10° and depends on the refractive indices of the reflecting prisms. The overall dimensions and the relative complexity of existing systems do not allow for easy embedding in a special chamber with the simulated operating conditions.

In this paper, the possibility of using point diffraction interferometry, based on single-mode optical fibers with subwavelength output aperture [11], for the measurement of ultrasmall angular displacement is considered for the first time, to the best of our knowledge. Experiments have shown that the accuracy of the measurements is about $0.01''$ in a range of $30''$ (the calibration range was restricted by the platform capabilities), which fully meets the requirements for characterization of the main mechanical properties of the platform. We present results for testing of the piezoelectric platform, developed for the telescope secondary mirror management.

2. EXPERIMENTAL SCHEME AND WORKING PRINCIPLE

Experiments were carried out on the point diffraction interferometer (PDI) stand described in [12]. A photo of the stand and the experimental scheme are shown in Figs. 1 and 2, respectively. The source of a spherical wave (SWS) is located in the center of curvature (i.e., at a distance of radius) of a spherical mirror (SM), and mounted on a tilting platform (TP). The SWS is a device for which the key elements are a single-mode optical fiber and a plane mirror with a hole in which the fiber is inserted. At the output of the fiber a diffractive spherical wave is formed; its angular width is within the first diffraction maximum $\pm\lambda/d$, where λ is the wavelength and d is the diameter of the exit aperture.

Since $d \approx 0.25$ μm, the operating wavelengths are 632 nm (He–Ne laser) and 532 nm (second harmonic of Nd:YAG laser), and the spherical wave occupies the half-space. Part of the wavefront incidents on the SM and after reflection (the working front) focuses on a plane mirror in close vicinity to the SWS and, being reflected from it, takes the form of a diverging wave that incidents on the CCD camera, interfering with part of the reference front. Angular displacements of the platform TP are produced by the piezo actuators, which are controlled by a digital-to-analog converter, integrated into the CCD camera, and an amplifier A.

The type of the interference pattern depends on the quality of the spherical mirror surface and on the configuration of the

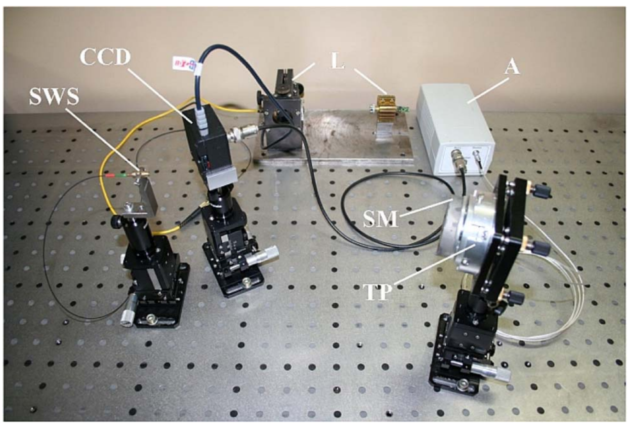

Fig. 1. Photo of the stand. SWS, source of a spherical wave, integrated into the flat mirror; CCD, digital camera; L, laser with the system of charging light to fiber; A, voltage amplifier for piezo actuator; SM, spherical mirror; TP, researched tilting platform.

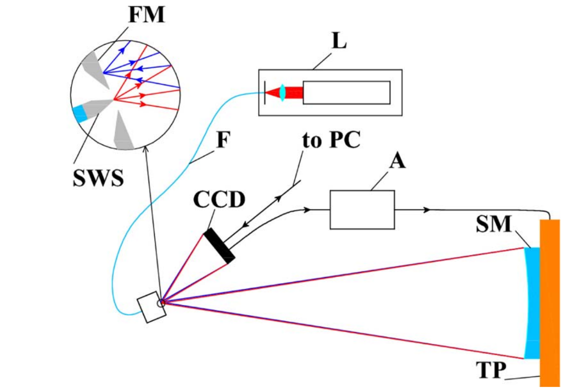

Fig. 2. Experimental schematic. FM, flat mirror; SWS, source of a spherical wave; CCD, digital camera, to PC, to a personal computer; F, single-mode optical fiber; L, laser with the system of charging light to fiber; A, voltage amplifier for piezo actuator; SM, spherical mirror; TP, researched tilting platform.

experiment, including the angular position of the platform on which the mirror is installed. The angular position of the platform determines the number of interference fringes, since, in fact, it determines the angle between the reference and working fronts. It should be noted that the mirror used in the experiments is a precision element, so its surface deformations result in minimal distortion to the interference fringes.

Since the interference pattern is formed as a function of the deformation of the wavefront—i.e., the difference between the reference and working fronts—after analysis, the angular position of the platform with a mirror can be restored. However, our main interest is the change in the angular position of the platform. This change can be calculated by comparing the functions of the wavefront deformation from two interferograms against the control voltage on the piezo actuator.

To construct the dependence of the platform rotation angle on the control voltage on the piezo actuator, a series of interferograms (up to 50 pcs) is recorded and synchronized with the changes in the control voltage. Figures 3(a)–3(c) show the interferograms corresponding to the zero, average, and maximum voltage. As seen from the images, the zero voltage corresponds to the interference pattern with 15 fringes, and the maximum corresponds to that with 42 fringes. The fact that the modern algorithms allow for an accurate determination of the position of the minimums, within 1/500–1/1000 of the fringe, qualitatively denotes the very high sensitivity and wide dynamic range (over 10^4) of the method.

As stated above, we need to restore the function of the wavefront deformation or its part, describing the inclination,

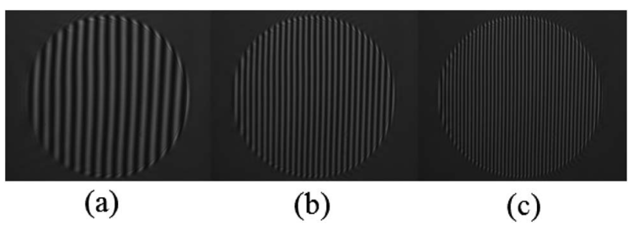

Fig. 3. Interferograms corresponding to (a) zero, (b) average, and (c) maximum voltage on the piezoelectric actuator.

in order to determine angles that correspond to interference patterns. The standard approaches to the interpretation of a single amplitude interferogram are methods of fringe tracking or methods of Fourier analysis. Since this problem does not require the restoration of the full surface, Fourier analysis is preferred, because it allows us to automate our calculations effectively.

Let us consider an ideal interference pattern that corresponds to the function of deformation, expressed in wavelengths, that includes only the slope:

$$I(x) = 1 + \cos(2\pi kx), \tag{1}$$

where $I(x)$ is the intensity distribution of the interference pattern, x is the spatial coordinate, and k is the angular coefficient, defined in wavelengths.

Let us consider a spatial frequency spectrum of the interference pattern, i.e., interferogram, consisting of strips of equal width:

$$\tilde{I}(\nu) = \delta(0) + 0.5\delta(\nu - k) + 0.5\delta(\nu + k), \tag{2}$$

where ν is the spatial frequency, and $\delta(\nu)$ is the Dirac delta-function. It is possible to mark out the central peak and two lateral secondary peaks, located at a carrier frequency k of the interferogram, which describes the slope of the deformation function of the wavefront.

The deformation function of the real interferogram includes not only tilt, but also other components of $\sigma(x)$, with substantially lower amplitudes rather than tilt. Equation (1) becomes

$$I(x) = 1 + \cos(2\pi(k + \sigma(x))x). \tag{3}$$

The spectrum of such an interference pattern can be written in the form [13]

$$\tilde{I}(\nu) = \delta(0) + 0.5\tilde{\Omega}(\nu - k) + 0.5\tilde{\Omega}^*(\nu + k), \tag{4}$$

where $\Omega(x) = \exp(2\pi i\sigma(x))$, $\tilde{\Omega}(\nu)$ is the Fourier transform, $*$ is the complex conjugation, and i is the imaginary unit. The kind of function $\sigma(x)$ is determined by the quality of the manufacturing mirror SM (SM is marked in Fig. 2), as well as the peculiarities of the spherical wavefront interference. Since the mirror is a high-precision element, and the centers of curvature of interfering fronts are separated by a small distance, $\sigma(x)$ is a smooth function, and $\tilde{\Omega}(\nu)$ has a shape of the peak with a maximum at the zeroth frequency, including frequency significantly lower than the frequency of the interference pattern, as well as high components of low amplitude determined by background noise. In addition, real interferograms are bounded by contours, the effect of which leads to a blurring of maxima and a little distortion of the background frequency band. Thus, the spectrum of the real interferogram recorded in accordance with the control scheme (Fig. 2) allows the determination of the position of the secondary maxima, corresponding to the slope of the wavefront deformation function.

A two-dimensional spectrum of real interferograms can be calculated using a fast Fourier transform (FFT). A typical spectrum of the interference patterns, recorded during the experiment, has a form [Fig. 4(a)] close to the ideal, but the central and secondary maxima are blurred [Fig. 4(b)]; in addition, there is a background band of spatial frequencies.

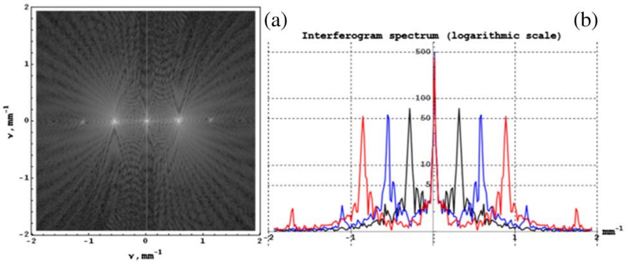

Fig. 4. (a) Two-dimensional spectrum of the measured interference pattern and (b) horizontal cross sections of the spectra corresponding to zero, average, and maximum voltage on the piezo actuator.

It is best to eliminate the background component in order to increase the stability of the determination of the secondary maxima of the interference patterns. Considering that the interferograms are obtained only by a change in the tilt angle, we can calculate the difference of the spectra of two interferograms. During this operation, the central peak and the background component are removed; the obtained function only contains information on the secondary maximum against the background of low-level noise. The best effect of this operation will be achieved, provided that the regions of the secondary maxima do not overlap. Assuming that interferograms are lined in ascending order of the inclination angle, the processing of a series of interferograms will be efficient when using the combination of the first interferogram with the second half of the series, and combinations of the last interferogram with the first half of the series.

The objective of the described processing step is the preliminary definition of interferogram carriers. Since this procedure is, in fact, the task of finding a global extreme, it is advisable to use the FFT procedure, allowing for calculating the sample of the spatial frequency spectrum. However, the result of the determination of the spectrum maxima using the FFT algorithm provides low accuracy, up to the case in which the carrier frequencies of neighboring interferograms cannot be distinguished. Thus a step of more precise definition of carriers is necessary.

In the process of formation and refinement of the vectors of carrier frequencies, it is convenient to use spectrum sample indices created from the FFT as coordinates. In this case, the sampling resolution of the spectrum is $\Delta\nu = 1$, so the sampling resolution of the interferogram in accepted conventional coordinates is $\Delta x = 1/N$, where N is the number of sample points.

The possibility to further clarify the location of extrema follows from the Nyquist–Shannon sampling theorem.

Let us present the sampling the interference pattern in the form

$$I_{\text{sample}}(x) = I(x) \cdot \text{comb}(x/\Delta x), \tag{5}$$

where $\text{comb}(x/\Delta x) = \sum_{n=-\infty}^{+\infty} \delta(x/\Delta x - n)$ is the Dirac comb, and $I(x)$ is the continuous interference pattern. The spectrum of such a function is

$$\tilde{I}_{\text{sample}}(\nu) = \tilde{I}(\nu) \otimes \text{comb}(\nu/N). \tag{6}$$

It follows from Eq. (6) that the spectrum of a discrete function is a periodic function, and within the same period it is a spectrum of envelopes of the original sample. Thus, the spectrum of the interferogram sampling is a continuous function that allows one to clarify the carriers of interferograms, calculated on the FFT spectrum.

Carrier refinement using interpolation methods, as well as searching for the center of mass, does not give a good approximation, and in some cases completely destroys the verification process. Secondary maxima have the shape of a peak, and, therefore, the derivative of the spectrum undergoes a discontinuity; moreover, blurriness around the peak may have a complex asymmetrical shape. The most stable method under these conditions is the bisectional method. The values of the integral of the Fourier transform at each step of the method are calculated numerically based on a sample of the interference pattern without using the FFT.

Refined two-dimensional carrier frequencies k_x, k_y are obtained now in relative coordinates of the interferogram. To go to the coordinates associated with the platform TP (Fig. 2), we require information about the diameter D of a spherical mirror and the operating wavelength λ.

Given that the contour of the interference pattern, expressed as the pixel dimensions of the axes S_x, S_y, corresponds to the diameter D, the resolution Δx, Δy, being cast in the platform coordinates, can be expressed as follows: $\Delta x = D/S_x$, $\Delta y = D/S_y$. The spectral resolution in these coordinates is $\Delta \nu_x = S_x/(N_x D)$, $\Delta \nu_y = S_y/(N_y D)$, where N_x and N_y represent the sample size of the interferogram.

Furthermore, as mentioned above, the units of the deformation function, including their inclination, were set as wavelengths. Therefore, for the conversion of the angular coefficient to the metric coordinates, its value, expressed in wavelengths, should be multiplied by the wavelength λ. It is also necessary to consider the double multiplicity of the control scheme that uses the mirror.

Thus, the conversion of the carriers' vector is

$$k_x^m = k_x \frac{\lambda S_x}{2DN_x}, \qquad k_y^m = k_y \frac{\lambda S_y}{2DN_y}. \tag{7}$$

Equation (7) allows us to go to the coordinates of the platform and calculate the values of angles along the coordinate axes: $\alpha_x = \arctan(k_x^m)$ and $\alpha_y = \arctan(k_y^m)$. The last step is to calculate the change in the angle of the platform for all series of interferograms relative to the first interferogram:

$$\Delta \alpha_i = \sqrt{(\alpha_{0x} - \alpha_{ix})^2 + (\alpha_{0y} - \alpha_{iy})^2}, \tag{8}$$

where the index of 0 means the first interferogram of the series, the index i – ith interferogram.

3. EXPERIMENTAL RESULTS

Figure 5 shows the angular dependence of the mirror tilt against the voltage on the piezo actuator; this relationship is averaged over a series of 10 consecutive measurements. The vertical lines on the graph indicate the standard deviations. There is a high reproducibility of the measurement using the PDI method; the standard deviation from the average is about ~0.01″ with the PDI method.

There is a lack of hysteresis in the graph because the first point in every measurement in series was set to zero.

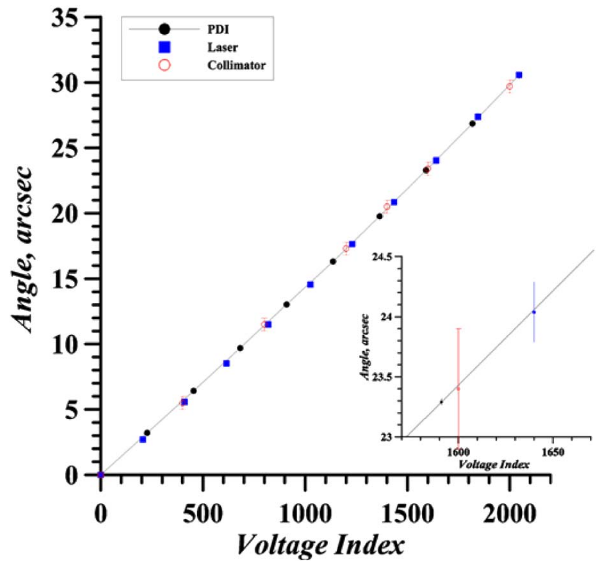

Fig. 5. Angular dependence of mirror tilt on the voltage of the piezo actuator that is averaged over a series of 10 consecutive measurements. Vertical lines on the graph indicate the standard deviations.

Since the parameters of the proposed method for determining the absolute value of the rotation angle are the values that are measured directly—the radius of curvature of the test mirrors, the distance between the SWS and the camera, the size of the CCD matrix, and the wavelength of the laser radiation—this method can be attributed to the "first principle."

Contributions to the relative bias include the following: the radius of curvature can be measured to an accuracy of a few hundredths of a millimeter (relative error 10^{-4}–10^{-5}), the distance between the SWS and a camera to tenths of a millimeter (relative measurement error 10^{-2}–10^{-3}), and the size of the CCD sensors (10^{-4}–10^{-3}) and the operating wavelength can be measured to a relative error of better than 10^{-5}.

The adequacy of the algorithm (i.e., the lack of global error) was confirmed by two methods. The first one is using an optical collimator with a value of graduation of 4″. The error of visual count was estimated at 0.5″. The second method can also be easily attributed to the "first principle"—a measurement of the displacement of the laser beam reflected from the flat mirror mounted on the investigated platform. The parameters of this measuring method are the distance between the mirror and a CCD and the size of the matrix.

Figure 5 shows the results obtained by all three methods. There is also a part of curves in a larger scale. As can be seen, the measurement results coincided within the statistical errors.

In practice, as long as the slope of the mirror is periodically changed upward and downward, it is necessary to find the platform hysteresis over the entire operating range. To this end, the following measurement algorithm was used. A series of interferograms was recorded while voltage changed from zero to maximum and from maximum to zero. The first interferogram in the series was set to the zero angle position, and all subsequent ones, including the zero voltage during the reverse motion, are set to the angle that is calculated according to the algorithm described above. Figure 6 shows the

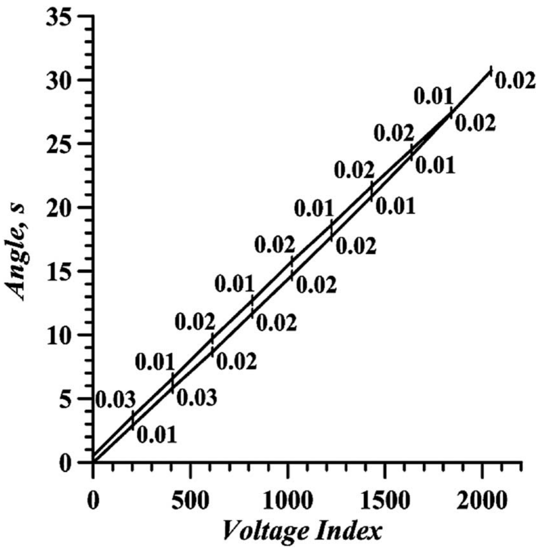

Fig. 6. Hysteresis curve, measured by the PDI method, for the tilting platform. Numbers on the graph indicate the standard deviations in arcseconds.

measurement results. As seen from the figure, there is a hysteresis loop; its angle value is about 1.5″.

4. CONCLUSIONS

This work proposes the method of measuring ultra-small angular displacement using point diffraction interferometry based on a single-mode optical fiber with a subwavelength output aperture. It has been experimentally shown that the sensitivity of the method can reach at least 0.01″ at the range of 30″. One would expect that by increasing the number of measurements in the series and creating special conditions for suppressing external vibration, the sensitivity of the method could be significantly improved. Due to the extremely small overall dimensions (a CCD camera has the greatest one) and fiber optic technology, the proposed instrument can be easily integrated into any device for *in situ* measurements of the small angle displacements. While carrying out such measurements, the laser controller and piezo actuator are installed outside, and only the SWS and a CCD camera are installed into the device chamber. The test spherical mirror is mounted on an investigated platform. Light from the laser is put into the device through a single-mode optical fiber, connected to a SWS via a FC/PC connector.

It should be noted that for practical applications, spherical mirrors with small numerical aperture (NA) $\ll 0.1$ can be used. In this case, a chipped single-mode optical fiber can be used as a source of the reference spherical wave, but in contrast to [14], it must be integrated into a single unit with a flat mirror. In the scanning process, the working wavefront is focused near the SWS, and performs a linear movement of more than the diameter of the silica fiber cladding.

Funding. Ministry of Education and Science of the Russian Federation (14.Z50.31.0007); Public Center for Physics and Technology of Micro and Nanostructures; Russian Foundation for Basic Research (RFBR) (13-02-00377, 14-02-00549, 15-42-02139).

REFERENCES

1. S. V. Kuzin, S. A. Bogachev, A. A. Pertsov, S. V. Shestov, A. A. Reva, and A. S. Ulyanov, “EUV observations of the solar corona with superhigh spatial resolution in the ARCA project,” Biol. Bull. Russ. Acad. Sci. **75**(1), 87–90 (2011).
2. http://www.optrotech.ru/eng/prod1-4-eng.php (last accessed 24 Sept. 2015).
3. C. Kuang, E. Hong, and Q. Feng, “High-accuracy method for measuring two-dimensional angles of a linear guideway,” Opt. Eng. **46**, 051016 (2007).
4. X. Bai, S. Cai, Y. Qiao, and M. Dai, “Small roll angle measurement based on auto-collimation and moiré fringe,” Proc. SPIE **7511**, 75110Z (2009).
5. C. Chen and P. D. Lin, “High-accuracy small-angle measurement of the positioning error of a rotary table by using multiple-reflection optoelectronic methodology,” Opt. Eng. **46**, 113604 (2007).
6. A. Su, H. Liu, and Q. Yu, “Multiple reflectors based autocollimator for three-dimensional angle measurement,” Proc. SPIE **9302**, 93023O (2015).
7. Z. Ge and M. Takeda, “A high precision 2-D angle measurement interferometer,” Proc. SPIE **4778**, 277–287 (2002).
8. Z. Ge and M. Takeda, “High-resolution two-dimensional angle measurement technique based on fringe analysis,” Appl. Opt. **42**, 6859–6868 (2003).
9. M. Ikram and G. Hussain, “Michelson interferometer for precision angle measurement,” Appl. Opt. **38**, 113–120 (1999).
10. W. Zhou and L. Cai, “Interferometer for small-angle measurement based on total internal reflection,” Appl. Opt. **37**, 5957–5963 (1998).
11. N. I. Chkhalo, A. Y. Klimov, V. V. Rogov, N. N. Salashchenko, and M. N. Toropov, “A source of a reference spherical wave based on a single mode optical fiber with a narrowed exit aperture,” Rev. Sci. Instrum. **79**, 033107 (2008).
12. M. V. Svechnikov, N. I. Chkhalo, M. N. Toropov, N. N. Salashchenko, and M. V. Zorina, “Application of point diffraction interferometry for middle spatial frequency roughness detection,” Opt. Lett. **40**, 159–162 (2015).
13. K. A. Goldberg and J. Bokor, “Fourier-transform method of phase-shift determination,” Appl. Opt. **40**, 2886–2894 (2001).
14. G. E. Sommargren, “Diffraction methods raise interferometer accuracy,” Laser Focus World **32**, 61–71 (1996).